

A Quantum-Mechanical Map for Bonding and Properties in Solids

Jean-Yves Raty, Mathias Schumacher, Pavlo Golub, Volker L. Deringer, Carlo Gatti, and Matthias Wuttig*

A 2D map is created for solid-state materials based on a quantum-mechanical description of electron sharing and electron transfer. This map intuitively identifies the fundamental nature of ionic, metallic, and covalent bonding in a range of elements and binary compounds; furthermore, it highlights a distinct region for a mechanism recently termed “metavalent” bonding. Then, it is shown how this materials map can be extended in the third dimension by including physical properties of application interest. Finally, it is shown how the map coordinates yield new insight into the nature of the Peierls distortion in phase-change materials and thermoelectrics. These findings and conceptual approaches provide a novel avenue to tailor material properties.

Materials with rationally controlled properties play important parts in the development of new and advanced technologies. Thermoelectrics, which convert waste heat into electricity, rely on the interplay of thermal and electric conductivity;^[1] phase-change materials (PCMs) for emerging neuromorphic^[2] or photonic^[3] applications exhibit an electrical and optical property contrast between amorphous and crystalline phases. All these properties can be traced back, to a significant extent, to the nature of interatomic bonding in materials.

Phenomenological descriptions of bonding in solids have been useful for centuries. Even to the nonscientist, the term “metal” implies reflective, ductile, electrically conducting

solids; a “semiconductor” has a narrow bandgap across which electrons can be excited by light; these classifications are therefore based on measurable, macroscopic properties. A fingerprint of five coexisting identifiers was recently used to define a concept termed “metavalent” bonding (MVB):^[4,5] metavalent solids show i) moderate electronic conductivity ($\approx 10^2$ – 10^4 S cm⁻¹); ii) increased coordination numbers incompatible with the (8–N) rule for semiconductors; iii) large optical dielectric constants, ϵ_∞ ; iv) large bond polarizability, as measured by Born effective charges, Z^* ; and v) large lattice anhar-


monicity, as measured by the Grüneisen parameter, $|\gamma_{TO}|$. In terms of conductivity and coordination numbers, metavalent solids are therefore located between the covalent and metallic regimes—but they are distinctly different from both because they show anomalously large response properties^[5] and a unique bond-breaking mechanism^[4] not observed in either covalent or metallic solids. This definition based on a set of observable properties directly led to a revision of the “resonant bonding” model (which had previously been widely used to describe the bonding in PCMs^[6]) by showing that the response properties of PCMs are fundamentally different from those of resonantly bonded benzene and graphite.^[5]

Dr. J.-Y. Raty
CESAM and Physics of Solids
Interfaces and Nanostructures, B5
Université de Liège
B4000 Sart-Tilman, Belgium

Dr. J.-Y. Raty
UGA
CEA-LETI
MINATEC campus, 17 rue des Martyrs, F 38054 Grenoble
Cedex 9, France

M. Schumacher
Institute for Theoretical Solid State Physics
RWTH Aachen University
52056 Aachen, Germany

Dr. P. Golub
Department of Mechanical Engineering
National University of Singapore
9 Engineering Drive 1, Singapore 117575, Singapore

 The ORCID identification number(s) for the author(s) of this article can be found under <https://doi.org/10.1002/adma.201806280>.

Dr. V. L. Deringer
Department of Engineering
University of Cambridge
Cambridge CB2 1PZ, UK

Prof. C. Gatti
CNR-ISTM
Istituto di Scienze e Tecnologia Molecolari
c/o Dipartimento di Chimica
Università degli Studi di Milano
via Golgi 19, Milano 20134, Italy

Prof. C. Gatti
7 Istituto Lombardo Accademia di Scienze e Lettere
via Brera 28, Milano 20121, Italy

Prof. M. Wuttig
Institute of Physics IA
RWTH Aachen University
52074, Aachen, Germany
E-mail: wuttig@physik.rwth-aachen.de

Prof. M. Wuttig
Peter Grünberg Institute (PGI 10)
Forschungszentrum Jülich
52428 Jülich, Germany

DOI: 10.1002/adma.201806280

To make the next, necessary step beyond such phenomenological models, one needs to understand the quantum-mechanical origins of bonding. Computational methods are widely used to (approximatively) solve Schrödinger's equation and describe the electronic wavefunction with increasingly high confidence, both in gas-phase molecules and in extended systems.^[7] Once this wavefunction is known, it allows to determine spatial distribution, localization, kinetic energy, and other properties of the electron, thereby providing numerical tools to quantify the bonding.^[8] Relationships of such descriptors with the empirical but powerful concepts of (operative) chemistry have been discussed and successfully exploited.^[9]

Here, we now combine the property-based and the quantum-mechanically based perspective to derive a holistic view of bonding in solids, and then show how this theoretical framework directly leads to novel design rules for materials with interesting properties. We analyze a range of elements and compounds: first, with a standard density-functional theory (DFT) approach to bring the Kohn–Sham wavefunctions to self-consistency; then, with a Hartree–Fock (HF)-like expression to compute the electron pair density, which describes the correlated motion of electrons (Supporting Information). The electronic density in the simulation cell is partitioned into so-called domains or basins Ω_i around the individual nuclei in the domain overlap matrix (DOM) method. DOM analyses have been routinely done for gas-phase molecules, but only very recently extended to the realm of plane-wave DFT and periodic systems.^[10] We note at the outset that DFT tends to over-delocalize electrons, whereas HF behaves in the opposite way, but these effects do not qualitatively affect our conclusions.

The DOM analysis yields a pair of simple descriptors that make it possible to classify or fingerprint any given solid-state material. First, we compute the net charge of an atom, Q_i , by integrating over its basin Ω_i and comparing to the free reference atom: doing so allows us to assess electron transfer, which is expected to be large in ionic solids (idealized example: Na^+ and Cl^- in table salt) but small otherwise. Second, we compute the delocalization index for a pair of atoms, $\delta(\Omega_i, \Omega_j)$, which yields the number of electron pairs exchanged or shared between them. Thus, $\delta(\Omega_i, \Omega_j)$ provides a physical measure of a property that classical models associate with covalency, and it is amenable to comparison with formal bond orders. A full pair of electrons shared between neighboring atoms corresponds to the Lewis picture of a single covalent bond. (Our y -axis is defined such that it gives the number of electrons; note that some authors prefer to report $\delta(\Omega_i, \Omega_j)$ directly and thus the number of electron pairs.)

We now use these descriptors as coordinates to draw a 2D materials map, which is shown in **Figure 1**. To appreciate its explanatory power, we first discuss archetypes of textbook bonding mechanisms and their location in this map. At the bottom and to the right, NaCl and MgO are generic examples of ionic bonding; the computed degree of electron transfer (0.87 and 1.71e, respectively) approaches the formal picture of Na^+ and Mg^{2+} ions. Looking at covalent solids, we find 1.83 electrons shared for diamond, approximating the Lewis electron-pair bond picture. In all cases, these limits are not reached completely: there is a very small covalent contribution even in NaCl , and there is some valence electron localized on each

atom in diamond (albeit no transfer, due to symmetry). The latter aspect becomes more obvious when moving down the fourth main group: diamond-type Si, Ge, and Sn show gradually less electron sharing, concomitant with their increasingly metallic nature. Binary compounds do exhibit electron transfer, but its extent is small in covalent systems and intermetallics, say TiAl . Clear chemical relationships can be observed in the map; e.g., the homologous III–V semiconductors, AlN , AlP , and AlAs , are close to one another; the largest change occurs between the first and second long periods (going from AlN to AlP) due to the different sizes of the valence p-orbital in N and P, as discussed by Burdett.^[11] The map also recovers the conventional wisdom that the transition between covalent and ionic bonding is gradual: this is best seen for the isovalent III–V compounds such as GaN and AlSb , where $\approx 1.5e$ (roughly half of the “cation” valence electrons) are transferred, concomitant with gradually decreasing covalency (y -axis). Finally, we can locate textbook examples of metallic bonding in the map: for example, Na shares only 0.2e (that is, it shows very little yet clearly nonzero covalency), as is characteristic for bonding via delocalized electrons.^[9a] This makes the metallic regime clearly distinct from nonbonded interactions, the latter being much closer to zero: as one example, a previous analysis for an $\text{Ar}\cdots\text{Ar}$ dimer yielded a delocalization index of only 0.013e (in the convention we use here, this corresponds to 0.026e shared).^[8d] In short, the map in Figure 1 identifies the archetypes of ionic, covalent, and metallic bonding in distinctly different and physically meaningful regions.

Previous “materials maps” date back to the iconic van Arkel triangle,^[12] which is widely found in textbooks, and to empirical structure maps for semiconductors based on tabulated orbital radii.^[13] We also mention a recently introduced 2D map that analyzes bonding in molecular systems.^[14] Perhaps the most closely related to the present work is an electronic-density-based study by Mori-Sánchez et al., using “density flatness” (a measure for metallicity), charge transfer (ionicity, similar to the present x -axis), and the molecular character as descriptors for the fundamental bonding mechanisms.^[15] The use of a “map” has been suggested in 2008 to identify candidate PCMs,^[16] but has been severely limited to a qualitative (and dichotomic “PCM”/“no PCM”) classification of materials, and again based on tabulated orbital radii from which heuristic proxies are constructed for “hybridization” and ionicity.^[16] This concept was later extended using DFT-based descriptors, which are sensitive to atomic structure.^[17] However, in all these studies, a crucial aspect has been missing: namely, a rigorous link between a compound's location in the 2D map on the one hand and its physical properties (as relevant for applications) on the other hand. Such a link would make it possible not only to classify bonding in materials, but to exploit the quantitative bonding information for materials design.

To create this link, let us look more closely at the central region of the map in Figure 1—which lies in between the three archetypal mechanisms, without clearly belonging to one of them, and is populated by materials as well (green symbols in Figure 1). One obvious explanation would be that the bonding nature in these materials is a superposition of existing archetypes. For example, hydrogen bonding may have van der Waals, ionic, and covalent contributions, strongly dependent on the

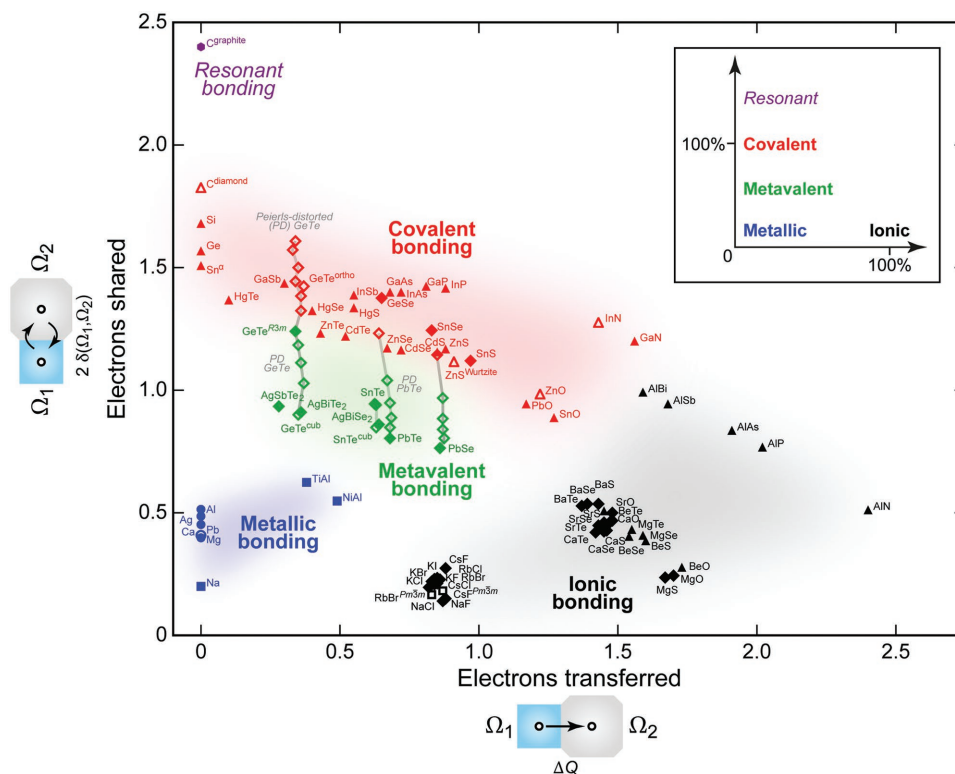


Figure 1. A 2D map of electronic interactions and bonding in materials. The amount of electrons transferred (*x*-axis) and shared between neighboring basins (*y*-axis) is computed using quantum-topological methods; they serve as quantitative measures for the ionic and covalent characters, respectively. We here consider elemental and binary phases of main-group elements, adding examples of transition metals, intermetallics, and ternary phases (Table S1, Supporting Information); however, the concept is applicable to any solid that can be treated with our computational tools. Symbols indicate structure types: “ sp^3 ”- (tetrahedrally) bonded solids are shown as triangles, distorted and ideal rocksalt-type (octahedrally coordinated) structures as diamonds, body-centered ones as squares, and close-packed metal structures as circles. Filled symbols denote thermodynamically stable phases (at zero temperature); open symbols denote metastable phases. For GeTe, SnTe, PbTe, and PbSe, additional structural intermediates have been generated along the Peierls distortion coordinate (gray lines as guides to the eye). The sketch in the inset summarizes the qualitative conclusions drawn from this map: we consider $2\delta(\Omega_1, \Omega_2) = 2$ to correspond to the sharing of a full electron pair, and therefore label this as “100%.” Resonantly bonded graphite sheets exhibit more than this one electron pair shared between the atoms; metavalent materials have distinctly less.

distance and nature of the acceptor atom;^[18] still, the associated physical properties (e.g., the O–H stretch frequency) change gradually and continuously between the respective limits. In sharp contrast, the MVB materials studied here show a rapid change and anomalously large values for three independent properties. To visualize and analyze this, we now extend the concept of our map into a third dimension, thereby including in the picture numerical values not just for bonding but also for those properties that define MVB (as discussed above). Such 3D maps, as shown in **Figure 2**, clearly reveal that such simultaneously and anomalously large properties are not found anywhere else within the space of our 2D map. Combining previous phenomenological, property-based evidence^[4,5] and the present quantum-mechanical study, it seems to emerge that MVB is a fourth bonding mechanism beyond the “big three” (ionic, covalent, and metallic).

Interest in MVB materials stems from their diverse technological applications, which are directly enabled by properties.^[19] Beyond its fundamental nature, **Figure 2** therefore suggests a blueprint to tailor the properties of MVB materials. For example, it was suggested that bonding in chalcogenides is closely interwoven with a lattice instability, leading to large

Grüneisen parameters.^[20] Our 3D plot (**Figure 2d**) now shows that this anomaly is uniquely linked to MVB—more specifically, to the border between MVB and metallic bonding. This provides a recipe to identify candidate thermoelectrics:^[21] move to MVB materials that border on metals, at around ≈ 0.8 electrons shared. While our map currently contains elements and binary compounds, its extension to ternaries is anticipated to reveal more candidate materials, given that a way can be found to localize the various contacts between different species within the 2D map. To illustrate this, we included in **Figures 1** and **2** selected ternaries such as $AgSbTe_2$ (see Table S1 in the Supporting Information), where we obtained the 2D coordinates by numerically averaging over values for Ag–Te and Sb–Te bonds.

All three *z*-axis quantities in **Figure 2b–d** are so-called response properties: they do not relate to conventional bond characteristics (such as the localization and delocalization of electrons), but rather to the unconventional way in which the bonds respond to external stimuli. In this light, it is interesting to mention recent studies on the electron organization of many-electron systems in the context of linear response theory.^[22] They highlight the profound connection between variances in local electronic position and the momentum operators and the

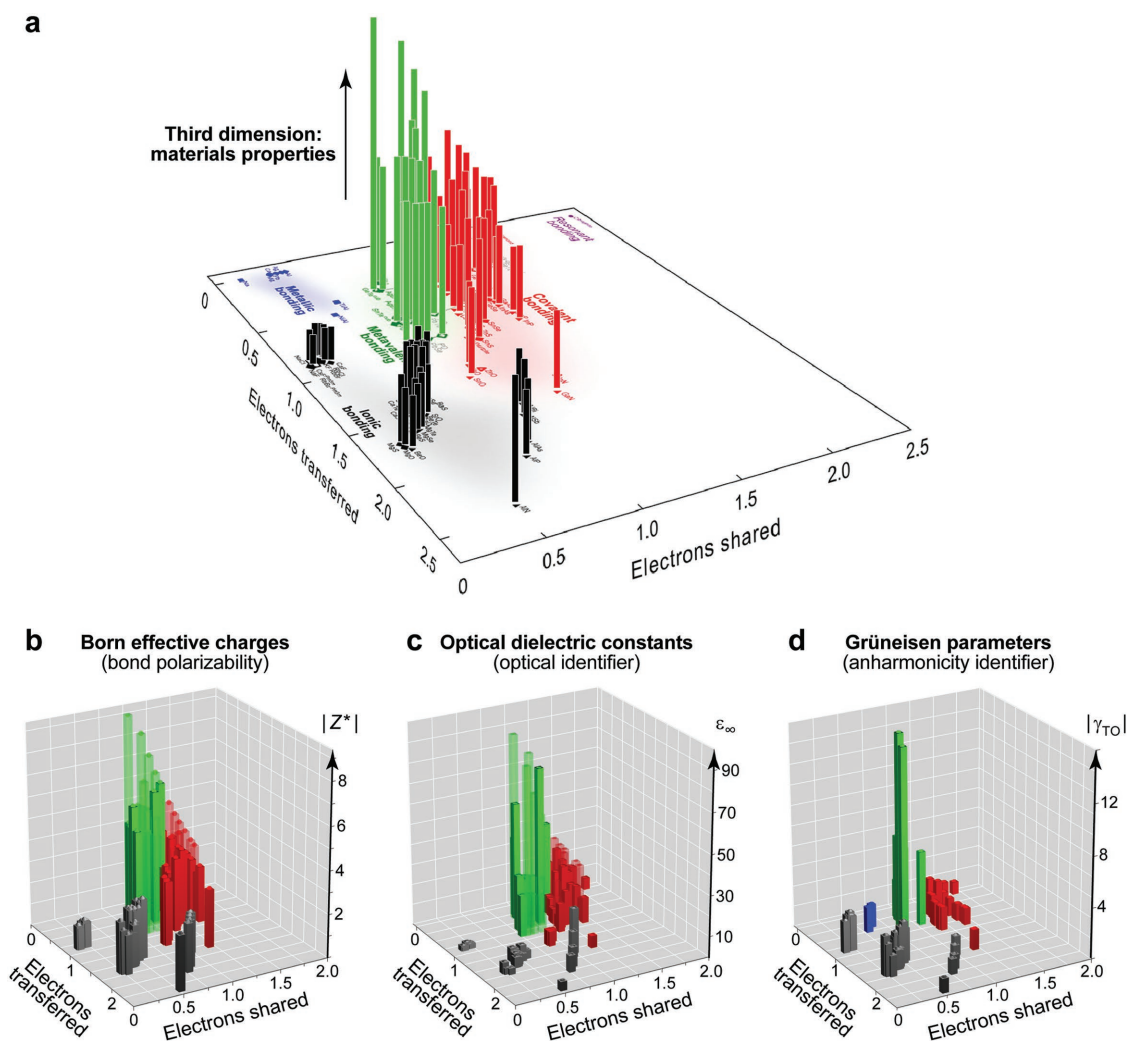


Figure 2. 3D maps defining design rules for materials with desired properties. The base plane is defined as in the 2D map (Figure 1) and quantifies electrons transferred and shared, respectively. Extending this map in the third dimension (as sketched in (a)), we quantify: b) Born effective charges, Z^* ; c) dielectric constants, ϵ_∞ ; and d) absolute transverse optical (TO) mode Grüneisen parameters, $|\gamma_{TO}|$, for binary compounds. Ionic materials are shown in black, covalent in red, and metavalent in green (with structural intermediates as semitransparent bars; see the Supporting Information for details). Metavalent bonding is characterized by unusually high values of all three indicators (green bars), and the 3D plots presented here allow to identify these trends across all of composition space. To design thermoelectrics, for example, one will navigate the base plane to regions of large lattice anharmonicity (d)).

optical conductivity tensor—that is, between electron (de)localization in real and momentum space on the one hand, and the experimentally observable spectroscopic and conductivity properties on the other hand. Our study emphasizes the dramatic role such connections may play in a peculiar case of bonding, namely, MVB.

The bonding descriptors used to define the map coordinates in Figures 1 and 2 can also shed new light on a long-standing issue in the structural study of MVB materials.^[23] Many of them crystallize in the rocksalt type (with ideal octahedral coordination of atoms) but some, prominently GeTe, show a small distortion that gives rise to three moderately shorter and three moderately longer bonds. This is referred to as a Peierls distortion (PD). In Figure 3, we analyze several structures with gradually varied degree of distortion, including stable α -GeTe and its undistorted cubic form. This allows us to mechanically

understand the transition between covalent (left-hand side) and metavalent (right-hand side) regimes. The progressive Peierls distortion induces a redistribution of electrons between short Ge–Te and long Ge–Te bonds, which become stronger and weaker, respectively (Figure 3a). However, the *average* amount of electrons shared is almost invariant; in other words, the total number of electrons forming bonds in crystalline GeTe is unaffected by the Peierls distortion. In the ideal cubic phase, ≈ 1 electron is shared between each of the six neighbors (which is half an electron pair, thus half the covalent limit, and typical of MVB; Figure 1). Still, even in the most strongly distorted structures (at low $R_{\text{short}}/R_{\text{long}}$) there remains non-negligible sharing in the longer bonds. This suggests the absence of any bond/no bond dichotomy: shorter and longer Ge–Te interactions are both associated with “true” bonds and are parts of the same body, with only the repartitioning of electron pairs varying. The

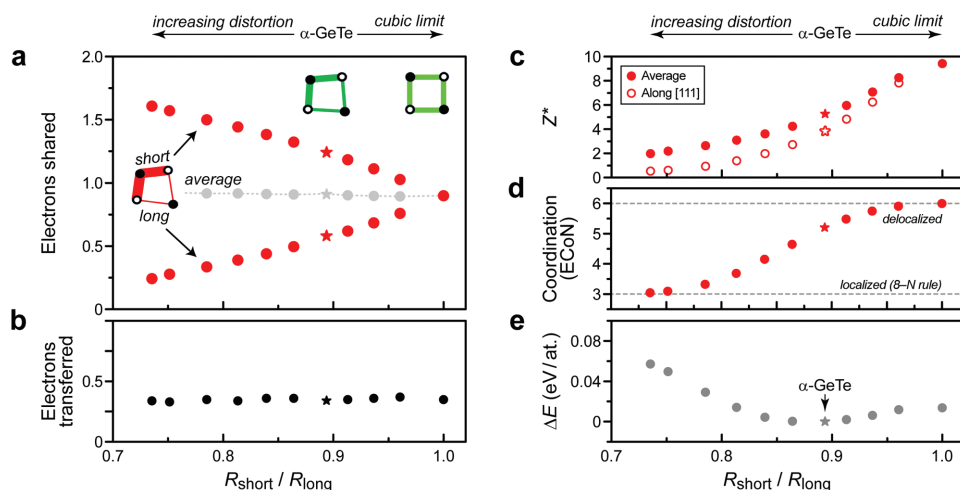


Figure 3. Mechanism of the Peierls distortion in materials as described by the quantum-based indicators that span our map. We analyze a series of GeTe structures that are gradually distorted along [111]. We quantify the degree of Peierls distortion (which is largest on the left-hand side) through the ratio of shorter and longer interatomic distances; both become equal in the limit of the ideal, undistorted rocksalt type (“cubic limit”). Left: a,b) The number of electrons shared and transferred (corresponding to the y - and x -coordinates in Figure 1, respectively). The Peierls distortion does not affect the amount of electrons transferred (i.e., the ionicity; panel (b)), but it does affect the distribution of electrons shared (panel (a)). Sketches for an “ABAB” ring fragment indicate the evolution of electron sharing and structural variation with the gradual variation of the Peierls distortion. Right: From top to bottom, we present different bonding characteristics and how they are affected by the Peierls distortion: c) the Born effective charges, providing a measurable indicator for the onset of MVB, given as average (filled symbols) and projected on the [111] direction where the effect of distortion is most relevant (open symbols); d) the effective coordination number, quantifying the gradual departure from the 8– N rule; e) the energy cost associated with the distortion, relative to α -GeTe, which is very small overall.

number of electrons transferred (Figure 3b) is unaffected by the Peierls distortion and small overall, dismissing the possibility for substantial ionic contributions to the bonding in this case. Turning to properties once more, the Peierls distortion is concomitant with an electronic instability of which the chemical bond polarizability is indicative (Figure 3c). The competition between localization and delocalization is reflected in a gradually changing effective coordination number (ECoN; Figure 3d), taking noninteger values between the extreme cases of three-fold coordination in the limit of strong distortion (in line with the 8– N rule, and typical for covalent semiconductors), and sixfold coordination in the cubic limit, again moving from the localized (covalent-like) to the delocalized (metallic-like) regime which is characteristic of MVB.^[5] The Peierls distortion appears to be decisive in achieving this delicate balance, especially as its energetic cost is very small (Figure 3e). Accordingly, small Peierls distortions are frequently encountered in MVB systems.

The data in Figure 3 suggest a route toward the design of properties (and thereby, ultimately, of “tailored” MVB materials) if one achieves control over the Peierls distortion. This could be done by strain, alloying, creating defects, or nanostructuring (moving along the horizontal axis in Figure 3 and modifying the ECoN as plotted in Figure 3d), and this directly allows to tune the properties—increasing thermoelectric efficiency, for example. It also explains how the amorphous phases of PCMs, in which the Peierls distortion becomes extremely large and directionally blurred,^[24] lose these anomalous properties, in turn creating the electronic and optical property contrast that is exploited in device applications.

In conclusion, we have presented a 2D materials map, based on quantum-mechanical analyses, which intuitively identifies the fundamental bonding mechanisms in solids. Extending this

map into the third dimension by including physical properties of application interest, we have provided evidence that metavalent bonding cannot be described by any combination of the three “textbook” mechanisms—it therefore constitutes a fourth fundamental bonding mechanism by accepted definitions. Our work opens up a conceptually new avenue for materials design: by searching for desired properties in a 3D space and then mapping this back onto the 2D plane of bonding, allowing scientists to navigate structural and composition spaces and to identify promising target materials.

Supporting Information

Supporting Information is available from the Wiley Online Library or from the author.

Acknowledgements

J.-Y.R. acknowledges computational resources provided by the CÉCI funded by the F.R.S.-FNRS under Grant No. 2.5020.11 and the Tier-1 supercomputer of the Fédération Wallonie-Bruxelles, infrastructure funded by the Walloon Region under grant agreement no. 1117545. J.-Y.R. acknowledges support from the Communauté française de Belgique through an ARC grant (AIMED 15/19-09). M.S. acknowledges computational resources provided by JARA-HPC (projects JARA0150, JARA0176, and JARA0183) and additional computing time provided by Prof. R. Mazzarello (Institute for Theoretical Solid State Physics, RWTH Aachen University). V.L.D. acknowledges a Leverhulme Early Career Fellowship and support from the Isaac Newton Trust. C.G. acknowledges partial support by the Danish National Research Foundation (Center for Materials Crystallography, DNRF93). This work was supported by Deutsche Forschungsgemeinschaft (DFG) through SFB 917

“Nanoswitches.” Moreover, the research leading to these results has received funding from the European Union Seventh Framework Programme (FP7/2007-2013) under grant agreement no. 340698, as well as the Excellence Initiative (Distinguished Professorship).

Conflict of Interest

The authors declare no conflict of interest.

Keywords

materials design, multivalent bonding, phase-change materials, thermoelectrics

Received: September 28, 2018

Revised: October 27, 2018

Published online: November 26, 2018

- [1] G. J. Snyder, E. S. Toberer, *Nat. Mater.* **2008**, *7*, 105.
- [2] C. D. Wright, Y. Liu, K. I. Kohary, M. M. Aziz, R. J. Hicken, *Adv. Mater.* **2011**, *23*, 3408.
- [3] M. Wuttig, H. Bhaskaran, T. Taubner, *Nat. Photonics* **2017**, *11*, 465.
- [4] M. Zhu, O. Cojocaru-Mirédin, A. M. Mio, J. Keutgen, M. Küpers, Y. Yu, J. Y. Cho, R. Dronskowski, M. Wuttig, *Adv. Mater.* **2018**, *30*, 1706735.
- [5] M. Wuttig, V. L. Deringer, X. Gonze, C. Bichara, J.-Y. Raty, *Adv. Mater.* **2018**, *30*, 1803777.
- [6] a) G. Lucovsky, R. M. White, *Phys. Rev. B* **1973**, *8*, 660; b) J. Robertson, K. Xiong, P. W. Peacock, *Thin Solid Films* **2007**, *515*, 7538; c) K. Shportko, S. Kremers, M. Woda, D. Lencer, J. Robertson, M. Wuttig, *Nat. Mater.* **2008**, *7*, 653.
- [7] R. Dronskowski, *Computational Chemistry of Solid State Materials*, Wiley-VCH, Weinheim, Germany **2005**.
- [8] a) A. D. Becke, K. E. Edgecombe, *J. Chem. Phys.* **1990**, *92*, 5397; b) R. F. W. Bader, *Atoms in Molecules: A Quantum Theory*, Oxford University Press, Oxford, UK **1994**; c) B. Silvi, A. Savin, *Nature* **1994**, *371*, 683; d) X. Fradera, M. A. Austen, R. F. W. Bader, *J. Phys. Chem. A* **1999**, *103*, 304; e) C. Gatti, *Z. Krist.* **2005**, *220*, 399; f) *Modern Charge Density Analysis* (Eds: C. Gatti, P. Macchi), Springer, Dordrecht, The Netherlands **2012**.
- [9] a) B. Silvi, C. Gatti, *J. Phys. Chem. A* **2000**, *104*, 947; b) F. Feixas, E. Matito, J. Poater, M. Solà, *Chem. Soc. Rev.* **2015**, *44*, 6434; c) M. Rahm, *J. Chem. Theory Comput.* **2015**, *11*, 3617.
- [10] a) A. I. Baranov, M. Kohout, *J. Comput. Chem.* **2011**, *32*, 2064; b) P. Golub, A. I. Baranov, *J. Chem. Phys.* **2016**, *145*, 154107.
- [11] J. K. Burdett, *Chemical Bonds: A Dialog*, John Wiley & Sons, Chichester **1997**.
- [12] a) A. E. van Arkel, *Moleculen En Kristallen*, Van Stockum, Den Haag, The Netherlands **1941**; b) L. C. Allen, *J. Am. Chem. Soc.* **1992**, *114*, 1510; c) W. B. Jensen, *J. Chem. Educ.* **1995**, *72*, 395.
- [13] a) J. C. Phillips, J. A. van Vechten, *Phys. Rev. Lett.* **1969**, *22*, 705; b) J. St. John, A. N. Bloch, *Phys. Rev. Lett.* **1974**, *33*, 1095.
- [14] M. Rahm, R. Hoffmann, *J. Am. Chem. Soc.* **2016**, *138*, 3731.
- [15] P. Mori-Sánchez, A. Martín Pendás, V. Luaña, *J. Am. Chem. Soc.* **2002**, *124*, 14721.
- [16] D. Lencer, M. Salinga, B. Grabowski, T. Hickel, J. Neugebauer, M. Wuttig, *Nat. Mater.* **2008**, *7*, 972.
- [17] M. Esser, V. L. Deringer, M. Wuttig, R. Dronskowski, *Solid State Commun.* **2015**, *203*, 31.
- [18] S. J. Grabowski, *Chem. Rev.* **2011**, *111*, 2597.
- [19] a) M. Wuttig, N. Yamada, *Nat. Mater.* **2007**, *6*, 824; b) V. L. Deringer, R. Dronskowski, M. Wuttig, *Adv. Funct. Mater.* **2015**, *25*, 6343.
- [20] S. Lee, K. Esfarjani, T. Luo, J. Zhou, Z. Tian, G. Chen, *Nat. Commun.* **2014**, *5*, 3525.
- [21] M. Cagnoni, D. Führen, M. Wuttig, *Adv. Mater.* **2018**, *30*, 1801787.
- [22] A. A. Astakhov, V. G. Tsirelson, *Int. J. Quantum Chem.* **2018**, *118*, e25600.
- [23] Bonding in these materials has been studied, although with somewhat different focus, using crystal orbital Hamilton population (COHP) analysis (that is, in terms of bonding and antibonding orbital interactions): a) U. V. Waghmare, N. A. Spaldin, H. C. Kandpal, R. Seshadri, *Phys. Rev. B* **2003**, *67*, 125111; b) M. Wuttig, D. Lüsebrink, D. Wamwangi, W. Welnic, M. Gilleßen, R. Dronskowski, *Nat. Mater.* **2007**, *6*, 122.
- [24] J.-Y. Raty, W. Zhang, J. Luckas, C. Chen, R. Mazzarello, C. Bichara, M. Wuttig, *Nat. Commun.* **2015**, *6*, 7467.